Search for a heavy neutrino and right-handed W of the left-right symmetric model in pp collisions at $\sqrt{s}$=7 TeV

D. Tlisov* on behalf of CMS collaboration
Institute for Nuclear Research RAS
Moscow, Russia

Abstract

This Note describes the first search for signals from the production of right-handed W_R bosons and heavy neutrinos N_ℓ ($\ell = e, \mu$), that arise naturally in the left-right symmetric extension to the Standard Model, with the CMS Experiment at the LHC using the 7 TeV pp collision data collected in 2011 corresponding to an integrated luminosity of 5 fb^{-1}. No excess over expectations from Standard Model processes is observed. For models with exact left-right symmetry (the same coupling in the left and right sectors) we exclude the region in the two-dimensional parameter space that extends to (M_{W_R}, M_{N_ℓ}) = (2500 GeV, 1700 GeV).

1 Introduction

The left-right (LR) symmetric extension to the Standard Model model [1, 2, 3] is attractive because it naturally explains the parity violation seen in weak interactions as a result of spontaneously broken parity. The model necessarily incorporates additional $W_R^\pm$ and Z' gauge bosons and heavy right-handed neutrino states N_ℓ and thus can also explain the smallness of the ordinary neutrino masses through the see-saw mechanism [4]. In this paper we present the results of the search for heavy neutrinos and the associated heavy gauge bosons of the minimal LR symmetric model using the Compact Muon Solenoid (CMS) detector at the LHC.

The strength of gauge interactions of $W_R^\pm$ bosons is described by the coupling constants g_R. Strict LR symmetry leads to the relation $g_L = g_R$ at M_{W_R}, which will be assumed throughout this paper. To simplify our study, we further assume that the mixing angles ($W_R - W_L$, $Z' - Z$, and $N_\ell - N_{\ell'}$) are small. The existing experimental limit on the W_R mass is in the range $739 - 768$ GeV and depends on the heavy neutrino mass (the smaller number corresponds to the case when all three N_ℓ have masses smaller than M_{W_R}) [5].

2 Heavy neutrino production and decay

We consider the leading production reaction at the LHC: $pp \to W_R + X \to N_\ell + \ell + X$. The right-handed neutrino decays into a charged lepton $\ell^\pm$ and an off-shell W_R^* which subsequently decays into a pair of quarks which hadronize into jets (j). As shown in Figure 3 this produces the final state

$$W_R \to \ell_1 N_\ell \to \ell_1 \ell_2 W_R^* \to \ell_1 \ell_2 jj \quad (\ell = e, \mu), \tag{1}$$

where ℓ_1, ℓ_2 have the same flavor.

*e-mail: dtlisov@cern.ch

A unique feature of the heavy neutrino production and decay process is that it has a two-dimensional resonance structure. The distributions of the variables $M_{\ell\ell jj}$ and $M_{\ell_2 jj}$ should exhibit rather narrow peaks, with the reconstructed width of $\mathcal{O}(100\ GeV)$ for the W_R mass peak and $\mathcal{O}(50\ GeV)$ for the width of the N_ℓ mass peak. In this analysis, we assume that only one type of heavy neutrino, predominantly coupled to either the electron or muon flavor, will be accessible at LHC energies with the other N_ℓ masses too heavy to produce. However, the case with degenerate N_ℓ masses does not differ significantly, as the opening of an additional decay channel for the W_R would decrease not only the lepton channels but also the quark channels.

Our search is characterized by the W_R and N_ℓ masses, which are allowed to vary independently. We note that the reaction used in the analysis can also proceed if $M_{N_\ell} > M_{W_R}$, but we neglect this possibility due to the relatively small cross section when compared to the dominant production mechanism.

Since QCD does not distinguish between left- and right-handed particles, the k-factor calculation is similar to the W and W' production k-factors [6]. In these calculations, made with the FEWZ program [7], α_s is taken at the W_R mass which results in a k-factor that slowly decreases as a function of M_{W_R}, from 1.33 at $M_{W_R} = 500$ GeV to 1.26 at $M_{W_R} = 2$ TeV (can be approximated by a straight line in this range).

We use PYTHIA [9], with default CTEQ6L1 parton distribution functions [10], for the signal event generation and calculation of cross sections. PYTHIA 6.4 includes the LR symmetric model with the standard assumptions mentioned above. We also study relevant background samples generated using PYTHIA, ALPGEN [11], and MADGRAPH [12].

3 Physical objects reconstruction and event selection

In this analysis we primarily reconstruct electrons, muons and jets, although we also examine photons and the missing transverse energy in the event for selected background studies. We collect the events used in this analysis through single electron or photon and single muon triggers with thresholds that depend on the instantaneous luminosity.

We reconstruct electron candidates offline starting by associating electromagnetic clusters in the ECAL with transverse energy $E_T > 40$ GeV with a track in the tracker and apply standard identification and isolation criteria optimized for electrons with energies of hundreds of GeV. The ECAL cluster for each electron candidate must be spatially matched to a reconstructed track in the central tracking system in both η and ϕ. Electron candidates must deposit most of its energy in the ECAL and relatively little in the HCAL ($H/E < 5\%$), and also have a shower shape consistent with that of an electromagnetic shower. The electron candidate cluster should be isolated from other energy deposits in the calorimeter and from reconstructed tracks in the central tracking system. More information about electron reconstruction and identification in CMS during this running period can be found in [13].

The muon identification strategy is based on both the muon detectors and the inner tracker, as described in [14, 15]. We require $p_T > 30$ GeV/c for both muons, where each muon is identified as a "global muon" with at least 10 hits in the silicon tracker. Additionally, at least one muon must pass tighter selection criteria where we look for a muon candidate with a transverse impact parameter with respect to the collision point of less than 2 mm, and the χ^2 per degree of freedom is below 10 for the global track fit. At least one hit from the pixel detector, and hits from at least two muon stations, must be used in the global fit. The tight muon (or either tight muon if both muons pass tight identification criteria) must also be matched to the muon trigger object. Muon identification requirements ensure good consistency between the measurements of the muon detector and the inner tracker and suppress muons from decay-in-flight of hadrons as well as shower punch-through. We suppress non-isolated muon backgrounds by summing the transverse momentum of tracks within $\Delta R < 0.3$ of the muon direction and requiring that the final p_T sum, ignoring the muon itself, is less than 10% of the muon p_T.

We reconstruct jets from calorimeter towers using the anti-kt clustering algorithm [16] with a cone of radius $R = 0.5$ and impose a minimum transverse momentum requirement of 40 GeV/c on the jet candidates. We apply standard jet identification procedures to suppress jets from calorimeter noise and beam halo, and we reject the event if either of the two highest p_T jet candidates fails identification criteria. The energy of reconstructed jets is corrected based on the results of simulation and data studies [17]. In the electron channel, and also in studies using $e\mu jj$ events, we do not consider jets if a valid electron candidate is found within the jet radius. As muons are not likely to fake jet signatures, we reject any muon found with $\Delta R(\mu, j) < 0.5$.

We rank the muons and jets in the event according to their transverse momentum and order the electrons according to their transverse energy, where the unique treatment of electrons reflects the dominant contribution of the ECAL energy to the electron energy/momentum measurement. We then select $W_R \to \ell N_\ell$ candidates using the two highest E_T/p_T same-flavor (e or μ) leptons, and the two highest p_T jets that satisfy the above criteria. As the $W_R \to \ell N_\ell$ decay tends to produce high momentum leptons, we further require $E_T(p_T) > 60$ GeV$(/c)$ for at least one of the lepton candidates. In the electron channel, we reject the event if no electron candidate is found in the ECAL barrel region ($|\eta| < 1.44$).

We limit contributions from Standard Model backgrounds by imposing requirements on the dilepton mass ($M_{\ell\ell}$) and the mass of the reconstructed W_R candidate ($M_{\ell\ell jj}$). Electroweak backgrounds, primarily from Z+jets, are suppressed by requiring $M_{\ell\ell}$ be above the Z mass. We optimize the $M_{\ell\ell}$ cut value as a function of (M_{W_R}, M_{N_ℓ}) to obtain the best expected limit via a single-bin Bayesian approach [20] with a flat prior. Based on our studies we require $M_{\ell\ell} > 200$ GeV, and note that we obtain the same minimum dilepton mass requirement when optimizing for W_R discovery.

The acceptance requirements for a candidate $W_R \to \ell N_\ell$ decay are that the decay products have sufficient E_T or p_T, are produced within the detector acceptance, and the lepton candidates do not overlap with jets. Additionally, the event fails acceptance requirements if $M_{\ell\ell}$ and $M_{\ell\ell jj}$ do not meet our minimum requirements. As $M_N \to 0$ (as well as when $M_N \to M_{W_R}$), it becomes more difficult to reconstruct the necessary four objects that meet all kinematic requirements. Furthermore, at low neutrino mass the $N_\ell \to \ell jj$ decay products tend to overlap, making it difficult to reconstruct leptons outside of the jet cone. We find that the signal acceptance is typically 70-80% at $M_N \sim M_W/2$ and drops to zero as we approach the M_N boundary conditions.

Provided the W_R candidate event meets all acceptance requirements, the ability to reconstruct four high p_T objects using the CMS detector is quite high. Reconstruction efficiency, including the trigger and lepton identification requirements, ranges between 75-80% in the muon channel, and 70-75% in the electron channel.

4 Backgrounds

The background for $W_R \to \ell N_\ell$ decay primarily consists of events from Standard Model processes with two real leptons, such as $t\bar{t}$ and Z+jets. It is also possible for jets to be misidentified as leptons, which allows QCD multijet processes to contribute background events.

We estimate the $t\bar{t}$ contribution using simulated events, normalizing it to the cross section measured by CMS [18]. We cross check this normalization using a sample of reconstructed $e\mu jj$ events in data and simulation. Based on the results of this study, we apply a small scale factor comparable with unity in addition to the cross-section normalization in order to account for the expected top background.

Our estimate of the Z+jets background contribution is based on observation of $Z \to ee, \mu\mu$ decays in simulation and data. We normalize the Z+jets contribution to the inclusive NNLO calculation [6, 7], and then rescale the expected distribution to data (accounting for background contributions) using the reconstructed dilepton mass region near the Z peak. We take the

remaining electroweak and top background estimates directly from simulation, as their small cross sections severely limit their impact on the background level.

We determine the QCD multijet background from data using an estimate of the lepton fake rate. For each channel, we examine a sample of dijet events in data in order to determine the lepton fake rate. For the electron channel this sample is selected using photon triggers with calorimeter isolation applied to enhance the purity of electron-like signatures, while for the muon channel we collect dijet events using the nominal analysis triggers. We increase the dijet sample purity by rejecting events with missing transverse energy above 20 GeV. We then apply the derived fake rate to a multijet sample, where the roughly 30% contribution from electroweak and top (as expected from simulation) are statistically removed via simulated event samples, to estimate the multijet background contribution to the $M_{\ell\ell jj}$ distribution.

5 Systematic uncertainties

We consider the following systematic uncertainties in this analysis, and summarize the systematic contribution per channel in Table 1.

- Jet energy scale and resolution: We scale the reconstructed jet energy up and down within the measured uncertainties [17] of about 1-7% per jet. We also smear the jet energy in the simulation to account for the uncertainty in jet resolution as measured in data. The normalization of the $t\bar{t}$ and Z+jets events to data imposes some constrants on this procedure, for this reason the size of this uncertainty is reduced for these samples.

- Electron and muon energy scale and resolution: based on the comparison of the M($\ell\ell$) distributions in the region of the Z peak in MC and data (two running periods), we investigate the impact of a variation on the measured electron E_T and muon P_T and a gaussian smearing of electron E_T and muon P_T.

- Electron and muon reconstruction, isolation, and identification: For the electron channel we obtain the uncertainty from a Tag&Probe study of $Z \to ee$ events in data and simulation. Taking into account the different P_t spectrum for electrons from W_R and N_e decay, and including the impact hadronic activity has on electron isolation quantities, we estimate a per-electron uncertainty of about 0.5%(1.1%) for barrel (endcap) region. For the muon channel, we obtain the uncertainty using a sample of $Z \to \mu\mu$ events.

- Trigger efficiency: For electron channel we measure it using the events collected with lower threshold double photon triggers (mostly prescaled) and use the statistical error of this measurement as a systematic uncertainty. We note that with our E_T cuts on electron candidates most of our events are well above the trigger turn-on region. For the muon channel, we vary the trigger efficiency based on a study of $Z \to \mu\mu$ events.

- Pileup: Superfluous pp collisions are included in the simulation to emulate the collision environment produced by the LHC. The uncertainty on the effects of pileup in simulation by varying the average number of collisions by ± 0.4 for Run A and ± 0.7 for Run B. item Background shape: We consider variations in the function used to describe the backgrounds, variations in the exponential slope obtained when fitting in different regions of $\ell\ell jj$ mass, as well as the nominal fit uncertainty for the simulated background distributions. We combine each of these uncertainties in order to estimate a total uncertainty related to the $M_{\ell\ell jj}$ background shape. This is done separately for each $M_{\ell\ell jj}$ bin (bin width is 200 GeV).

- Background normalization: we obtain an uncertainty for $t\bar{t}$ and Z+jets backgrounds based on scaling our expectations from simulated event samples to data. For the remaining backgrounds, we combine their cross section uncertainty with the CMS luminosity uncertainty.

- Statistical uncertainty from simulated samples: We obtain this uncertainty from the number of simulated background events that survive the full analysis selection.
- Theoretical uncertainties: We investigate the impact of modified initial and final state radiation, variations in the proton parton distribution function parameters, and factorization and scale variations using dedicated samples of simulated events.
- QCD background estimation: We apply our estimated fake rate to a separate three-jet sample and compare our predictions to a sample of reconstructed $e/\mu + jj$ events.

6 Results

We summarize the observed and expected number of events surviving our selection requirements in Table 2 and Table 3, and present the $M_{\ell\ell jj}$ distribution for events passing all cuts in Figures 2. We observe no excess beyond expectations from Standard Model processes.

We set upper limits using a multibin limit setting technique based on the RooStats package [19]. We use as a final variable the reconstructed four-object mass (m_{eejj} or $m_{\mu\mu jj}$) for masses above 600 GeV. The mass is collected in bins of width 200 GeV, comparable to the mass resolution for a right-handed W signal. The contributions from runs A and B for each mass range are treated as separate bins, to account for the different acceptances of the two analyses and properly account for the different rates of pileup in the two running periods. The background contributions to each bin are determined from the analytical shape fits applied to each background type.

Systematic uncertainties are included as nuisance parameters in the limit calculations.

We take the reconstruction and identification systematic uncertainties to be uncorrelated between the 2010 and 2011 analysis, while all other systematic uncertainties are considered correlated between 2010 and 2011. We use a Bayesian limit setting technique where the probing of the systematic uncertainty space is carried out using a Markov Chain Monte Carlo technique. The results of this limit setting were consistent with the result of the $\mathrm{CL_S}$ technique.

The 95% C.L. limits on the cross-section times branching fraction as function of M_N are estimated with a $\mathrm{CL_S}$ limit setting technique for the masses of W_R in the sensitivity region with a step of 100 GeV. The two example plots for different M_{W_R} are shown in Figure 3. Good agreement is seen between the observed and expected limits. These results can be used for the evaluation of different model assumptions than those considered above. For the model described above, we show the mass regions excluded in Figure 4, where we obtain these plots by comparing the observed (expected) upper limit and the expected cross section for each mass point. The limits extend to $M_{W_R} = 2500$ GeV, and exclude a wide range of heavy neutrino masses for M_{W_R} =2000 GeV. In addition to the 95% C.L. exclusion limits shown as a function of W_R and N_μ mass in Figure 4.

7 Conclusions

We have presented a search for right-handed bosons (W_R) and heavy neutrinos (N_e) of the left-right symmetric extension of the Standard Model. The background contribution from the top and electroweak processes is determined from simulated event samples and the expected rates are normalized to data whenever possible. The background from QCD multijet events is estimated from data. The uncertainty for the backgrounds is estimated using data-driven methods. We find that our data sample is in good agreement with expectations from Standard Model processes. We use a $\mathrm{CL_S}$ approach to set a limit on the W_R and N_ℓ masses that includes

Table 1: Summary of the systematic uncertainties, collected for each channel 2011 datasets where the magnitudes of each uncertainty are estimated following the procedure described in the text. The total errors in the bottom row are obtained by summing in quadrature all the relative uncertainties in a given column. The uncertainties on the total number of background events are derived taking into account the relative contribution of all background events after the full event selection, and the correlation of each systematic effect between the all background processes.

Electron Channel

Systematic Uncertainty	Signal eff.	$t\bar{t}$	Z+jets	QCD	Other bkgd
Jet Energy Scale	±0.3-9%	±10%	±2%	–	±5%
Jet Energy Resolution	±0-1%	±0.6%	±1%	–	±2%
Electron Energy Scale	±0.1%	±1.5%	±2%	–	±1.2%
Electron Energy Resolution	<0.1%	<0.1%	±0.5%	–	±0.5%
Electron Reco/ID/Iso	±4-13%	±2%	±5%	–	±8%
Trigger Efficiency	±1%	±1%	±1%	–	±1%
Pileup, runs A (B)	±2(11)%	±2(11)%	±2(11)%	–	±2(11)%
Background shape	–	±20%	±15%	±25%	±25%
Simulation statistics	±5-20%			–	
Background normalization	–	±9%	±3%	–	±6%
ISR/FSR	±1-3%	–	–	–	–
PDF	±8-40%	±0.4%	±0.4%	–	±9%
Fact./Ren. scale	0%	±7%	±5%	–	±8%
QCD estimate	–	–	–	±33%	–
Total	±16-49%	±30%	±21%	±42%	±34%

Muon Channel

Systematic Uncertainty	Signal eff.	$t\bar{t}$	Z+jets	QCD	Other bkgd
Jet Energy Scale	±0.3-13%	±9%	±3%	–	±8%
Jet Energy Resolution	±0-0.4%	±0.4%	±0.2%	–	±0.2%
Muon Energy Scale	±0-0.4%	±0.2%	±3.0%	–	±0.4%
Muon Reco/ID/Iso	±15-18%	±3%	±6.0%	–	±7%
Trigger Efficiency	±0.6-1.5%	±0.2%	±0.3%	–	±4%
Pileup	±0-0.4%	±0.2%	±1.0%	–	±2%
Background shape	–	±15%	±11%	–	±40%
Simulation statistics	±5-20%	–	–	–	–
Background normalization	–	±9%	±1%	–	±7%
PDF	±8-40%	±0.4%	±0.4%	–	±9%
Fact./Ren. scale, ISR/FSR	±1-2%	±7%	±5%	–	±8%
QCD estimate	–	–	–	±60%	–
Total	±18-50%	±21%	±14%	±60%	±44%

Table 2: Data statistics and signal/background yields after each stage of the event selection for the electron channel. Values displayed in the "Signal" column assume $M_{W_R} = 1800$ GeV and $M_{N_e} = 1000$ GeV.

	Data	Signal	Tot.Bg	$t\bar{t}$	Z+jets	QCD	Other
E0	8896	44	9028	969	7830	61	168
E1	6283	44	6234	779	5277	46	132
E2	5516	43	5478	762	4566	32	118
E3	311	42	311	192	92	13	14
E4	124	42	132	71	48	7	6

Key:

Designator	Meaning
E0	Two HEEP electrons, two jets with kinematic and ID requirements applied
E1	One electron with $p_t > 60$ GeV/c
E2	At least one electron in Barrel
E3	$M_{ee} > 200$ GeV
E4	$M_{eejj} > 600$ GeV

treatment of the systematic uncertainties as nuisance parameters. For models with exact left-right symmetry (the same coupling in the right sector) we exclude the region in the two-dimensional parameter space (M_{W_R}, M_{N_ℓ}) that extends to $M_{W_R} = 2500$ GeV.

This work was partly supported by the grant RFFI N10-02-00468.

References

[1] J. C. Pati and A. Salam *Phys. Rev. D* **10** (1974) 275.

[2] R. N. Mohapatra and J. C. Pati *Phys. Rev. D* **11** (1975) 366.

[3] G.Senjanovic and R.N.Mohapatra *Phys. Rev. D* **12** (1975) 1502.

[4] R. Mohapatra and G. Senjanovic *Phys. Rev. Lett.* **44** (1980) 912.

[5] D0 Collaboration *Phys. Rev. Lett.* **100** (2008) 211803.

[6] P.Nadolsky, "Theory of W and Z production", `arXiv:hep-ph/0412146`.

[7] R. Gavin, Y. Li, F. Petriello et al., "FEWZ 2.0: A code for hadronic Z production at next-to-next-to-leading order", `arXiv:1011.3540`.

[8] CMS Collaboration *JINST* **3** (2008) S08004.

[9] T.Sjostrand et al. *JHEP* **001-026** (2006). hep-ph/0603175.

[10] J.Botts et al. *Phys. Lett. B* **304** (1993) 159.

[11] M.L.Mangano, M.Moretti, F.Piccinini et al., "ALPGEN, a generator for hard multiparton processes in hadronic collisions", *JHEP* **0307:001** (2003). hep-ph/0206293.

[12] J.Alwall et al., "MadGraph/MadEvent v4: The New Web Generation", *JHEP* **09:028** (2007). 0706.2334.

Table 3: Statistics after each stage of the event selection for the muon channel. Values displayed in the "Signal" column assume $M_{W_R} = 1800$ GeV and $M_{N_\mu} = 1000$ GeV.

	Data	Signal	Tot.Bg	$t\bar{t}$	Z+jets	QCD	tW	VV
M0	23925	51	24072	1805	21910	6.7	65	285
M1	21769	50	21060	1603	19136	6.1	59	256
M2	13328	50	12862	1106	11531	2.7	46	176
M3	365	48	341	211	116	0.3	9	5
M4	164	48	152	81	65	0.2	4	2

Key:

Designator	Meaning
M0	Two muons, two jets with kinematic and ID requirements applied
M1	Single muon trigger requirement
M2	One muon with $p_t > 60$ GeV/c
M3	$M_{\mu\mu} > 200$ GeV
M4	$M_{\mu\mu jj} > 600$ GeV

[13] CMS Collaboration, "Electron reconstruction and identification at $sqrt(s)$=7 TeV", *CMS PAS* **EGM-10-004** (2010).

[14] CMS Collaboration, "Performance of CMS muon identification in pp collisions at $\sqrt{s} = 7TeV$", *CMS PAS* **MUO-2010-002** (2010).

[15] CMS Collaboration, "Search for Resonances in the Dilepton Distribution in pp Collisions at sqrt(s) = 7 TeV", *CMS PAS* **EXO-10-013** (2010).

[16] M. Cacciari and G. Salam and G. Soyez, "The anti-kt clustering algorithm", *JHEP* **04** (2008).

[17] CMS Collaboration, "Jet Energy Corrections Determination at 7 TeV", *CMS PAS* **CMS-PAS-JME-10-010** (2010).

[18] CMS Collaboration, " Measurement of the t t-bar Production Cross Section in pp Collisions at 7 TeV in Lepton + Jets Events Using b-quark Jet Identification", *Phys. Rev. D* **84:092004** (2011).

[19] L. Moneta, K. Belasco, K. Cranmer et al., "The RooStats Project", *PoS* **ACAT2010** (2010) 057, `arXiv:1009.1003`.

[20] I. Bertram, G. Landsberg, J. Linnemann, R. Partridge, M. Paterno and H.B. Prosper, "A Recipe for the construction of confidence limits", *Fermilab* **TM-2104** (2000),

`http://lss.fnal.gov/archive/test-tm/2000/fermilab-tm-2104.pdf` .

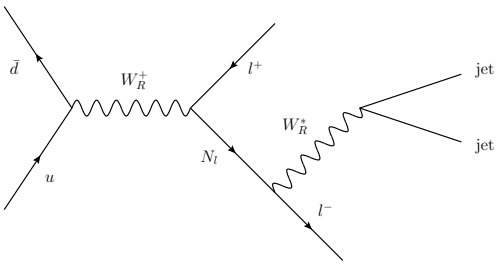

Figure 1: W_R and N_ℓ production and decay.

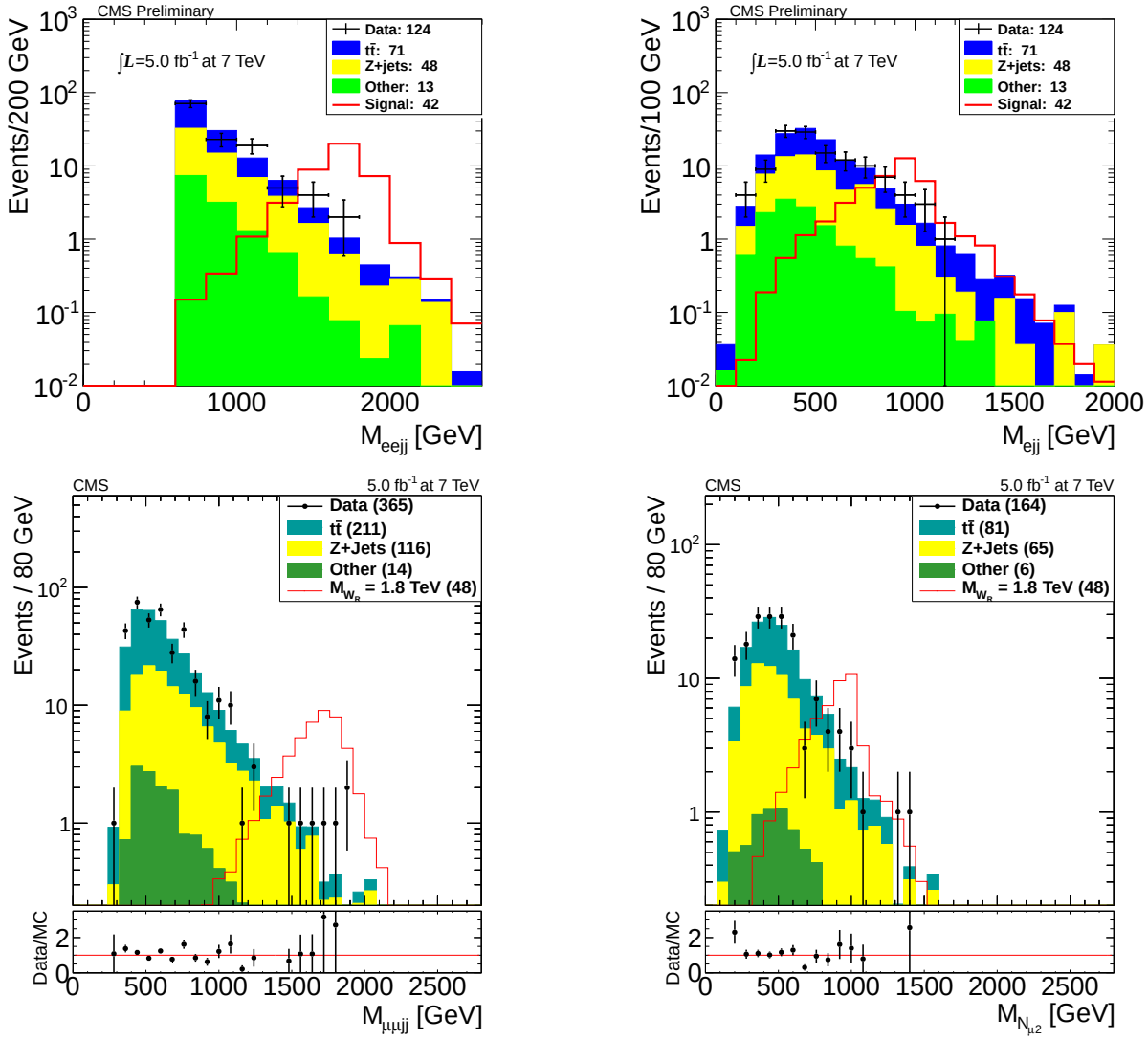

Figure 2: Distributions for events surviving event selection criteria, neglecting the four-object mass requirement, in the electron (top) and muon (bottom) channels using the 5 fb^{-1} collision data collected in 2011. The signal mass point M_{W_R} = 1800 GeV, $M_{N_{e(\mu)}}$ = 1000 GeV, is included for comparison.

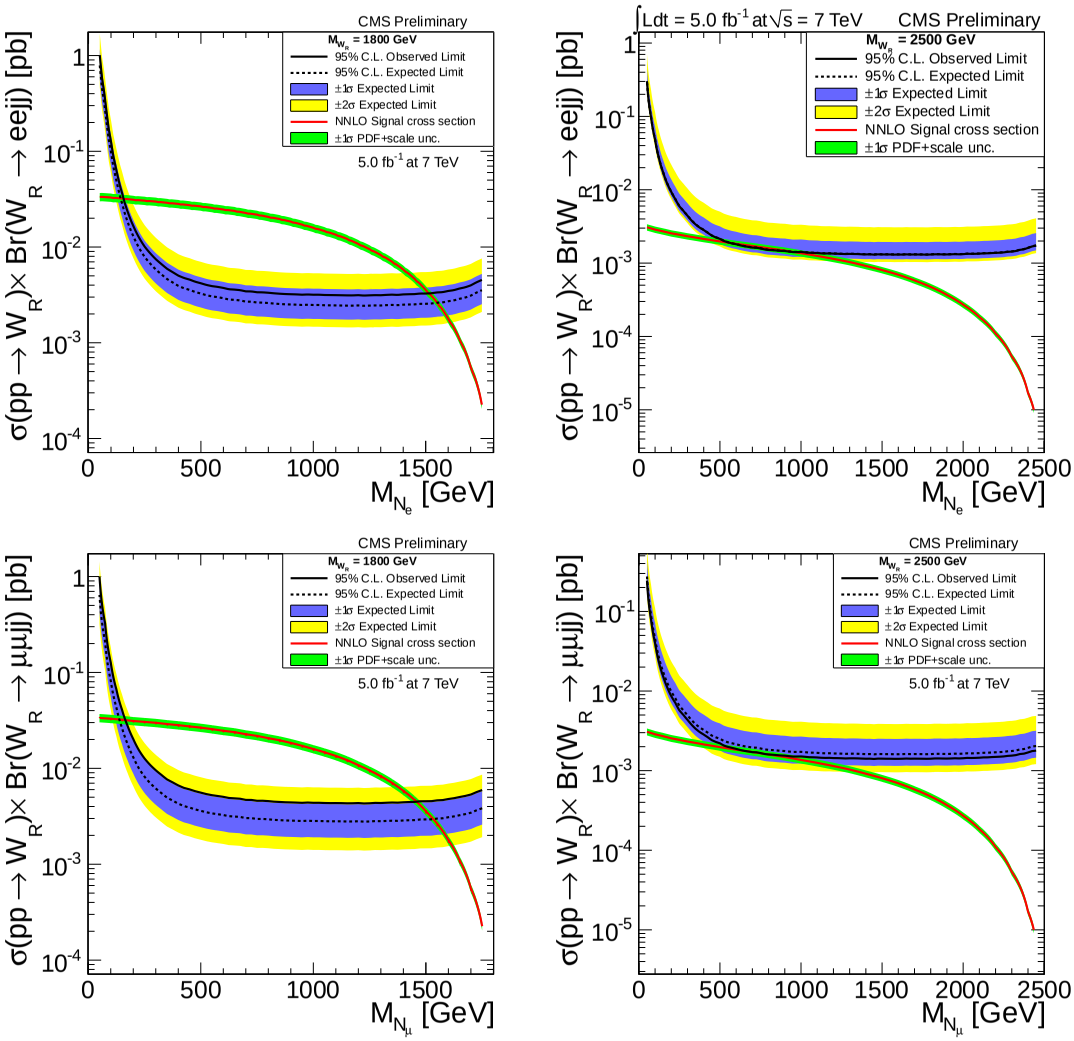

Figure 3: 95% C.L. exclusion plots for electron (top) and muon (bottom) channels, using the method described in the text, for a selection of M_{N_ℓ} and M_{W_R} hypotheses. Exclusion as a function of M_{N_μ} for $M_{W_R} = 1.8TeV$ (left), for $M_{W_R} = 2.4TeV$ (right).

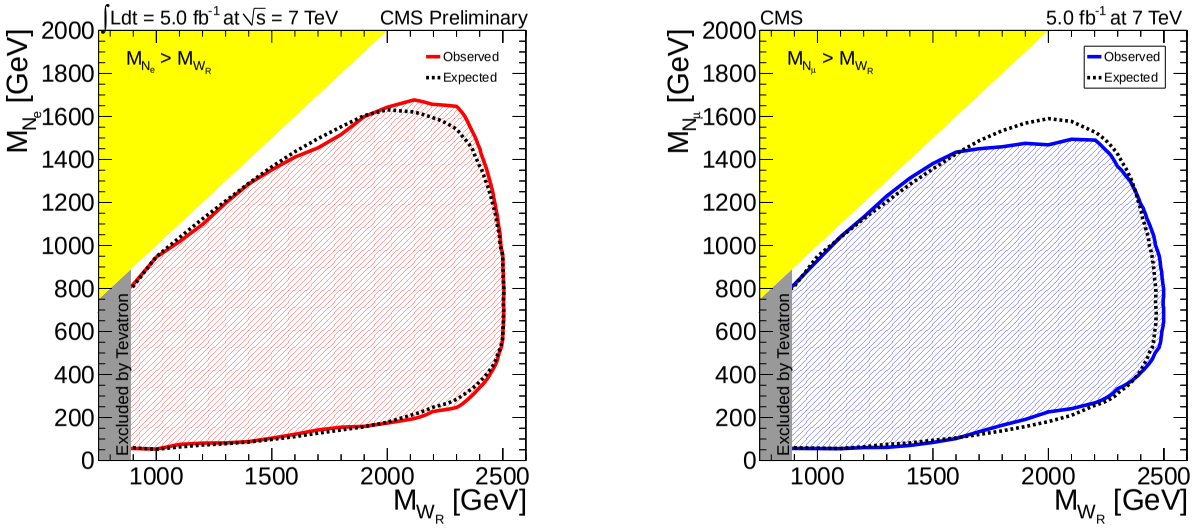

Figure 4: The 95% confidence level excluded (M_{W_R}, M_{N_ℓ}) region for the electron (left) and muon (right) channels.